Advances in Turbulence X
Proceedings of the Tenth European Turbulence Conference
H. I. Andersson & P.-Å. Krogstad (Eds.)

Three dimensional structure characterization and visualization in a turbulent boundary layer

B. Ganapathisubramani[1], E. Longmire[1], I. Marusic[1], T. Urness[2], V. Interrante[2]
[1]Dept. of Aerospace Engineering & Mechanics
[2]Dept. of Computer Science,
University of Minnesota, Minneapolis, MN 55455.
Contact address: *bugs@aem.umn.edu*

1 Introduction

For decades, researchers have worked towards developing a suitable model to represent turbulent boundary layers. Based on PIV experiments in the $x-z$ planes of a turbulent boundary layer, Adrian *et al.* [1] proposed a model based on a packet of "hairpin vortices" as a primary feature in turbulence transport and production (In this paper, streamwise, spanwise and wall-normal directions are along x, y, and z axes respectively). Based on stereo PIV data in $x-y$ planes, Ganapathisubramani *et al.* [2] concluded that these hairpin packets occupy a small percentage of the total area, yet contribute nearly 30% of the total Reynolds shear stress generated. Hence, the hairpin packets are a very important mechanism in turbulence production.

With single plane data, however, we cannot completely characterize the intensity or orientation of the vortices responsible for generation of Reynolds shear stress. For example, swirl strength (λ_{ci}, see Zhou *et al.* [3]) calculated from the imaginary part of the eigenvalue of a 2-D velocity gradient tensor, performs reasonably well at identifying vortex core locations but does not reveal their orientation. Hence, dual-plane stereo PIV experiments were performed and resulting datasets were used to retrieve the complete velocity gradient tensor. With the out-of-plane gradients provided by the dual-plane data, we can compute the complete swirl strength and the direction of the vorticity vector. We can also compute the instantaneous turbulence production term ($uw\frac{\partial U}{\partial z}$) and determine its relation to the vortex structures in the flow.

2 Experiment and methods

Experiments were performed in a boundary layer wind tunnel in a zero-pressure-gradient flow with freestream velocity $U_\infty = 5.9$ m s^{-1} and $Re_\tau = 1060$ ($Re_\tau = \delta U_\tau/\nu$, where δ is the boundary layer thickness, U_τ is the skin friction velocity). All quantities shown in this paper are normalized using U_τ and ν, and denoted with superscript $+$.

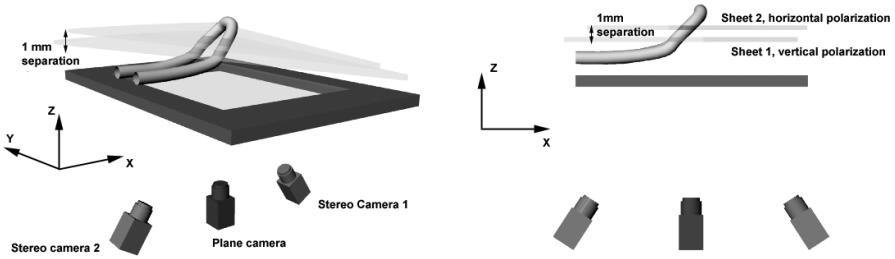

(a) (b)

Figure 1: (a) Perspective view (b) side view of the experimental setup

Two independent PIV systems capture data simultaneously in neighboring streamwise-spanwise planes separated by $\sim$ 1 mm (15 wall units) as shown in figure 1. System 1 is stereoscopic and provides all three velocity components over a plane illuminated by Sheet 1. System 2 uses a single camera to measure the streamwise and spanwise velocity components in the higher plane illuminated by Sheet 2. Simultaneous measurements are performed utilizing the polarization property of the laser sheets to isolate one plane to one set of camera/cameras (see Kahler & Kompenhans [4]). PIV data were captured in the log layer at $z^+ = 125$ (System 1) and $z^+ = 140$ (System 2). The single camera vector field from the upper plane in liaison with the stereoscopic data from the lower plane are then used to compute all velocity gradients in the lower plane. A second order central difference method is used to compute all in-plane gradients while a first order forward difference is used to compute the wall-normal gradients of the streamwise and spanwise velocities. Finally, the continuity equation is used to recover the wall-normal gradient of the wall-normal velocity.

3 Results

Figure 2 reveals a closer look into a region identified as a hairpin packet (outlined by the thick black line) by the algorithm described in [2]. Figures 2(a) and 2(b) reveals the instantaneous two-dimensional swirl strength (${\lambda^+}_{2D}$) at $z^+ = 125$ and $z^+ = 140$ respectively. These plots in tandem with wall-normal vorticity (${\omega^+}_z$ at $z^+ = 125$) shown in figure 2(c) reveal that 2-D swirl identifies regions swirling about an axis aligned with the wall-normal direction. A visual comparison of the swirl in the two planes indicates a forward tilt of most structures as they are offset in the positive streamwise direction in the upper plane. (This trend is observable in many pairs of planes, in particular when they are viewed in rapid succession). Figure 2(d) shows instantaneous production, $uw^+(\partial U^+/\partial z^+)$. Some locations of strong production coincide with swirling zones. Previous results indicated that regions of high Reynolds shear stress occurred within hairpin packets. Figure 2(d) shows highest production levels in the packets near the legs

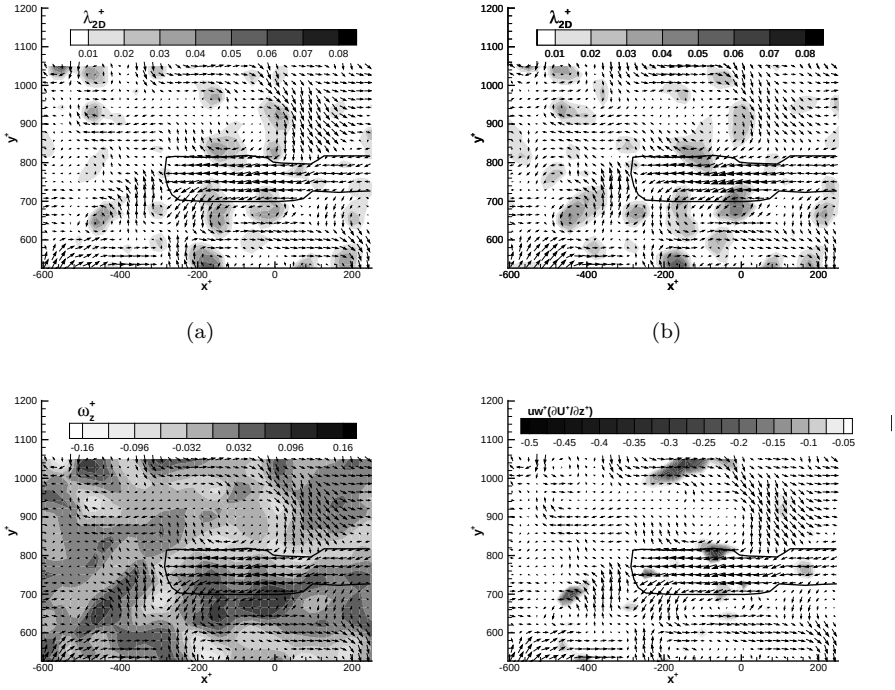

Figure 2: (*a*) $\lambda^+{}_{2D}$ at $z^+ = 125$, (*b*) $\lambda^+{}_{2D}$ at $z^+ = 140$, (*c*) Wall-normal vorticity ($\omega_z{}^+$) and (*d*) Instantaneous production $uw^+(\partial U^+/\partial z^+)$ at $z^+ = 125$.

of hairpins and in the heads.

Examination of 3-D swirl ($\lambda^+{}_{3D}$, computed using full velocity gradient tensor) fields indicates that $\lambda^+{}_{3D}$ identifies not only the hairpin necks angling across the plane but also additional regions not found by $\lambda^+{}_{2D}$. These regions coincide with smaller hairpin vortex heads that intersect the measurement volume or the seemingly streamwise legs of much bigger structures.

The inclination angle of vortex structures can be computed by determining the orientation of the vorticity vector. If the vector angle is computed at every point in the field, the results are noisy because of both measurement uncertainty and the fact that instantaneous vortex lines in a turbulent flow are not very organized. By contrast, computation of an average vorticity vector in a region identified as a vortex core by the swirl strength ($\lambda^+{}_{3D}$), leads to determination of the orientation of the vortex core. This orientation can then be interpreted as the local inclination of that vortex.

Figure 3(a) reveals the probability density function (*pdf*) of the inclination

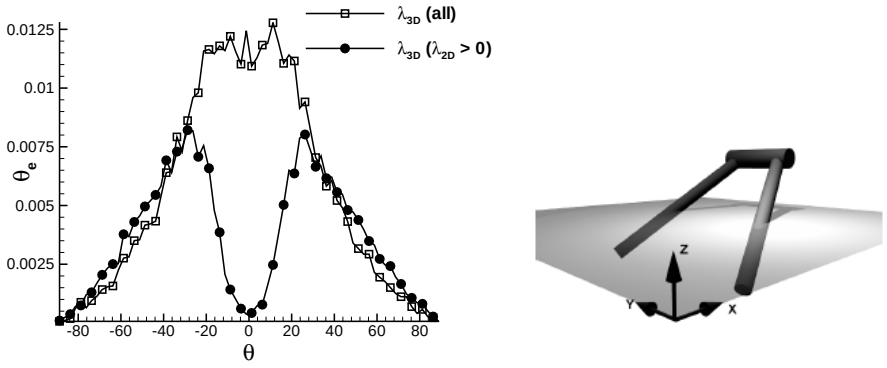

(a) (b)

Figure 3: (a) *pdf* of inclination angle (b) Schematic of hairpin structure

angle vortex cores make with the $x-y$ plane (θ_e). The angles were computed for all distinct regions of significant $\lambda^+{}_{3D}$. This distribution (square symbols) includes a wide range of structure angles at this z^+ location. Note that many structures have small inclination angles. Further study, including the investigation of the azimuthal angle made by the projection of the vorticity vector onto the $x-y$ plane with the x axis, reveals that most $\lambda^+{}_{3D}$ regions with small inclinations are spanwise structures indicative of heads of smaller hairpin vortices.

In order to obtain the inclination angles of cores that are not spanwise heads or streamwise legs, the average vorticity vector in isolated regions of $\lambda^+{}_{3D}$ including significant $\lambda^+{}_{2D}$ were computed. This additional criterion filters out spanwise and streamwise structures since $\lambda^+{}_{2D}$ does not capture them. The resulting *pdf* (filled circles in figure 3(a)) yields peaks at $\pm 25^\circ$. This suggests that most cores are inclined at 25° to the x-y plane with a resulting eddy inclination of 32°. A schematic of a representative hairpin is shown is figure 3(b).

The authors gratefully acknowledge support from the National Science Foundation through Grants ACI-9982274, CTS-9983933 and CTS-0324898 and the Graduate school of University of Minnesota.

References

[1] Adrian RJ, Meinhart CD, Tomkins CD 2000 *J. Fluid Mech.* **422**

[2] Ganapathisubramani B, Longmire EK, Marusic I 2003 *J. Fluid Mech.* **478**

[3] Zhou J, Adrian RJ, Balachandar S, Kendall TM 1999 *J. Fluid Mech.* **387**

[4] Kahler CJ & Kompenhans J 2000 *Exp. Fluids* **Suppl:** S70-S77